Vertical Tilts of Tropospheric Waves: Observations and Theory

WESLEY EBISUZAKI

Department of Geology and Geophysics, Yale University, New Haven, Connecticut

(Manuscript received 25 August 1989, in final form 4 February 1991)

ABSTRACT

The vertical tilts of planetary waves as functions of zonal wavenumber and frequency were examined by two methods. First, the vertical tilts were computed by a cross-spectral analysis of the geopotential heights at different pressures. This generally used technique was not as sensitive as a cross-spectral analysis of height and temperature at a single level. The two methods yield similar vertical tilts; however, the latter method had a smaller error that allowed us to find statistically significant tilts in the troposphere that the former method did not find.

In the midlatitude troposphere, the eastward-moving waves had a westward tilt with height, as expected. However, the westward-moving waves with frequencies higher than 0.2 day^{-1} showed statistically significant eastward vertical tilts. For a free Rossby wave, this implies that the Eliassen–Palm flux is downward along with its energy propagation. A downward energy propagation suggests an upper-level source of these waves.

It was proposed that the eastward-tilting waves were forced by the nonlinear interaction of stationary waves and baroclinically unstable cyclone-scale waves. The predicted vertical tilt and phase speed were consistent with the observations. In addition, simulations of a general circulation model were analyzed. In the control run, eastward-tilting waves disappeared when the sources of stationary waves were removed. This is consistent with our theory.

1. Introduction

In this paper, we calculated the vertical tilts of transient waves in the midlatitude troposphere using two methods. The results of the two methods are consistent with each other; although the commonly used method is less sensitive. Consequently, our results differ from earlier studies.

The vertical tilts were chosen for this study because they determine the following dynamical properties: vertical group velocity, vertical component of the Eliassen–Palm (E–P) flux, and meridional heat flux. When large-scale waves have a westward tilt, the waves transport heat poleward and the E–P flux is upward, which implies an upward energy propagation where $(U - c)$ is positive (U is the zonal wind and c is the phase speed of the wave). In addition, the ridges (troughs) of the temperature field are west of the corresponding ridges (troughs) of the height field. Eastward-tilting waves have the opposite properties.

A priori, one might expect that Rossby waves tilt westward with height. A major source of waves is baroclinic instability, and if the instability resembles either the Charney or Green modes (of the Charney problem), then the waves should tilt westward with height (e.g., Pedlosky 1987). Orography is another source of waves. One would expect that flow over a mountain would produce waves that would propagate energy away from the source. Since the source is at the surface and $(U - c)$ is positive, the E–P flux should be upward along with the energy flux. This, of course, implies a westward tilt with height. The land–ocean contrasts can also force waves. The sensible heat flux from the surface and the latent heat release occurs mainly in the lower levels, especially during winter. Therefore, one would expect an upward energy flux from these sources and westward-tilting waves.

With a cross-spectral analysis, we found that westward-propagating waves [$f > 0.2$ cycles per day (cpd)] had an eastward tilt in the troposphere. If these were free waves, then there must be an upper-level source of these waves. However, no obvious source was found. While the power contained by these waves were small, they were examined in detail because their vertical tilts were unexpected and unexplained.

2. Previous work

In this paper, we examined the vertical tilts of transient disturbances as functions of zonal wavenumber and frequency. Basic methods used to find the vertical tilts by frequency band are 1) compositing techniques, 2) EOF analysis, and 3) cross-spectral analysis. Madden and Speth (1989) used compositing to find the global structure of very large-scale waves. Their method selected westward-propagating waves with periods between 9 and 30 days. They found no vertical tilt in the northern midlatitude troposphere.

Corresponding author address: Dr. Wesley Ebisuzaki, Climate Analysis Center/NMC, W/NMC 51, Washington, D.C. 20233.

Pratt and Wallace (1976) used an EOF analysis to investigate the low-frequency vertical structure of tropospheric variability. By calculating the empirical orthogonal functions (EOFs) for the vertical structure, they found a few spatial modes that could explain large percentages of the vertical variability. They found that at scales typical of baroclinic instability ($k = 8$, $f = 0.3$ cpd), the EOFs tilt westward with height. The 5-day ultralong wave ($k = 1$, $f = 0.2$ cpd; see Salby 1984) was barotropic, and the long waves at low frequency ($k = 1, 2$; $f = 0.05$ cpd) had westward tilts.

Venne (1989) calculated the EOFs for the three-dimensional structure of the troposphere and stratosphere. He filtered the data into the zonal wavenumbers and frequencies associated with various ultralong waves and then determined the EOFs. The EOFs and the theoretical global normal modes agreed well. Venne found that the EOFs and a westward tilt height agree with the theory (Salby 1981) and energy-flux arguments. (The stratosphere has large effective dissipation rate due to radiative cooling. Since a normal mode cannot change its structure, energy must flow from regions of low dissipation to high dissipation, assuming the mode is stable. Hence, energy must flow into the stratosphere, and the normal mode must tilt westward in the troposphere.)

Finally, cross-spectral analysis has been used to find tilts. Typically, the geopotential height, Z, is decomposed into a time series of spherical harmonics or zonal waves (at a fixed latitude), and the cospectrum between the time series at different pressure levels is found. Analysis using spherical harmonics was reviewed by Madden (1979), who reported that the westward-propagating large-scale modes show little vertical tilt in the troposphere and lower stratosphere.

Cross-spectral analysis using zonal wavenumbers has the advantage of ignoring the meridional structure. Consequently, the analysis is not biased to ultralong waves or the tropics. Such analysis has been conducted by Sato (1977) for the stratosphere and Deland (1973), Bötteger and Fraedrich (1980), and Mechoso and Hartmann (1982) for the Southern Hemisphere. Deland (1973) found that the westward-moving waves had little phase tilt in the troposphere at 40° and 50°N. Bötteger and Fraedrich (1980) analyzed one year of observations for 50°N. The synoptic-scale eastward-moving waves had a westward tilt; the low-frequency (0.05 cpd) eastward-moving long waves had a westward tilt; and the westward-moving long waves had little tilt in the troposphere. Mechoso and Hartmann (1982) analyzed one Southern Hemisphere winter and obtained results similar to Bötteger and Fraedrich (1980).

3. Data

We used the compact disc subset of the National Meteorological Center's (NMC) gridpoint dataset (Mass et al. 1987) for our atmospheric data. This dataset contains twice-daily gridded values north of 20°N. We used 20 years of seasonal data (90 days per season) starting on 1 December 1964 and 1 June 1965 for the winter and summer data. Missing data were linearly interpolated. To avoid contamination by the annual cycle, the annual cycle was removed from the winter data by fitting the mean of the 20 winters to a parabola and removing this fitted mean from the data. The summer data were similarly filtered.

We also analyzed simulations of the NCAR Community Climate Model Version 1 (CCM1), a 12-layer 15-wavenumber resolution (rhomboidal 15) general circulation model [see Williamson et al. (1987) for a detailed description]. The first GCM simulation analyzed (GCM–CLIMO) is based on January insolation, January sea surface temperatures, and present orography (Williamson and Williamson 1987). The second simulation, GCM–FLAT, resembled GCM–CLIMO, except the whole globe is covered with a zero-elevation grassland. The grassland has an albedo of 0.15 and 0.34 to visible and near-ultraviolet light, respectively. In addition, the grassland has a fixed soil moisture; its latent heat flux is set 11% of what would be obtained if there were water instead of grasslands under the same conditions. The surface temperature was determined by a surface energy balance involving the incoming and outgoing radiative fluxes, the sensible heat flux, and the latent heat flux, with the assumption that the soil had zero heat capacity.

GCM–FLAT had no forced stationary waves because it lacks mountains and oceans. This simulation was used to help evaluate the role of orography in determining the wave structure. For GCM–CLIMO, we analyzed five 90-day "seasons" that were separated by 90-day intervals. In GCM–FLAT, four 90-day seasons separated by 30-day intervals were analyzed. The seasons were separated by 30- or 90-day intervals so that the analyzed periods were statistically independent.

4. Method of data analysis

Our analysis was made for 90-day seasons on a fixed latitude and pressure surface. For a given latitude, pressure, and fixed number of observations, a field such as the geopotential height can be written using a discrete Fourier transform as

$$Z(x, t) = \sum_{n=-N}^{N} \sum_{k=0}^{M} \tilde{Z}(\omega_n, k) \exp(2\pi ikx/L - i\omega_n t), \tag{1}$$

where $L = 2\pi \cos(\theta) R_{\text{earth}}$ is the circumference of the latitude circle. For our twice-daily analysis, the Nyquist frequency, ω_N, is 2π day^{-1}. Since a 256-point Fourier transform was used, $\omega_n = n\delta\omega$, where $\delta\omega$ is $2\pi/128$ day^{-1}.

With this representation, the variance was decomposed into eastward- and westward-traveling Fourier modes, or waves for short. (Our use of "waves" does not imply a normal mode structure.) We calculated $\tilde{Z}$ and $\tilde{T}$ by 1) interpolating the 180 twice-daily analyses onto 32 equally spaced points on the 50°N latitude circle, 2) removing the annual cycle, 3) Fourier transforming the data into zonal wavenumbers, 4) removing the time mean of the time series, and 5) Fourier transforming each time series. This procedure is equivalent to the space–time spectral and analysis of Hayashi (1982).

Our decomposition is sensitive to standing waves [e.g., $h(x)\sin(\omega t)$] because a standing wave will decompose into eastward- and westward-propagating waves of equal magnitude. This contamination is probably important for periods longer than about one week. The consequences of not removing the standing wave are discussed in section 6.

We determined the vertical tilt by two methods. First, the usual method of calculating the phase angle between the 200- and 500-mb $\tilde{Z}$ was used. From the phase angle, ϕ_Z, a direct measure of the vertical tilt as a function of zonal wavenumber and frequency is obtained. In addition, we calculated the phase angle between the heights and the temperatures (ϕ_T). This gives an indirect measure of the tilt.

Both methods require us to find the phase angle as determined from the transfer function H. For a two-variable system, H is

$$\tilde{Z}(500\text{ mb}, \omega, k) = H_Z(\omega, k)\tilde{Z}(200\text{ mb}, \omega, k) \quad (2)$$

$$\tilde{Z}(500\text{ mb}, \omega, k) = H_T(\omega, k)\tilde{T}(500\text{ mb}, \omega, k), \quad (3)$$

where $|H|$ is the gain, $\phi_Z = \arctan[\mathrm{Im}(H_Z)/\mathrm{Re}(H_Z)]$ is the phase angle between $\tilde{Z}(500\text{ mb})$ and $\tilde{Z}(200\text{ mb})$, and $\phi_T = \arctan[(\mathrm{Im}(H_T)/\mathrm{Re}(H_T)]$ is the phase angle between $\tilde{Z}$ and $\tilde{T}$. Positive ϕ_Z implies on eastward tilt with height. A positive ϕ_T implies that $\tilde{T}$ is shifted east of the $\tilde{Z}$, which, by the hypsometric equation, indicates that the lines of constant phase tilt eastward with height.

We could determine H_T by simply dividing $\tilde{Z}$ by $\tilde{T}$. However, noise would make the value nearly useless. Instead, our estimate of H is improved by averaging the estimates of several seasons. Next, the assumption is made that $H(\omega)$ changes slowly, that is, $H(\omega_i) \approx H(\omega_{i\pm1}) \approx H(\omega_{i\pm2})$; e.g., H was averaged in a small frequency window. By frequency averaging H, we lose some frequency resolution, but reduce the noise. Basically, we are averaging the transfer function in a frequency window of width $4\delta\omega$. With 20 seasons and 5 points in the frequency window, there are 100 independent estimates of H. The least-squares estimates of H are

$$\hat{H}_T = \sum_{i=1}^{100} (\tilde{T}_i^* \tilde{Z}_i(500\text{ mb})) \Big/ \sum_{i=1}^{100} |\tilde{T}_i|^2 \quad (4)$$

$$\hat{H}_Z = \sum_{i=1}^{100} (\tilde{Z}_i^*(200\text{ mb})\tilde{Z}_i(500\text{ mb})) \Big/ \sum_{i=1}^{100} |\tilde{Z}_i(200\text{ mb})|^2, \quad (5)$$

where $\hat{H}$ is the frequency-domain equivalent of the regression coefficient, and the complex coherence is the equivalent of the correlation coefficient

$$\gamma_T = \Big(\sum_{i=1}^{100} \tilde{T}_i^* \tilde{Z}_i(500\text{ mb})\Big) \times \Big(\sum_{i=1}^{100} |\tilde{Z}_i(500\text{ mb})|^2 \sum_{i=1}^{100} |\tilde{T}_i|^2\Big)^{-1/2}$$

$$\gamma_Z = \Big(\sum_{i=1}^{100} \tilde{Z}_i^*(200\text{ mb})\tilde{Z}_i(500\text{ mb})\Big) \times \Big(\sum_{i=1}^{100} |\tilde{Z}_i(500\text{ mb})|^2 \sum_{i=1}^{100} |\tilde{Z}_i(200\text{ mb})|^2\Big)^{-1/2},$$

where $|\gamma|^2$ is similar to the square of the correlation, $0 \leq |\gamma|^2 \leq 1$, and $|\gamma|^2 = 1$ implies a linear relationship.

The error bonds on $|H|$ and the phase angle are (Otnes and Enochson 1978)

$$|\hat{H}| - \hat{r} < |H| < |\hat{H}| + \hat{r}$$

$$\hat{\phi} - \Delta\phi < \phi < \hat{\phi} + \Delta\phi$$

$$\hat{r}_T^2 = \frac{2}{n-2} F_{2,2n-2}(1 - |\gamma_T|^2) \frac{\hat{S}_{Z(500\text{ mb})}}{\hat{S}_T}$$

$$\hat{r}_Z^2 = \frac{2}{n-2} F_{2,2n-2}(1 - |\gamma_Z|^2) \frac{\hat{S}_{Z(500\text{ mb})}}{\hat{S}_{Z(200\text{ mb})}}$$

$$\Delta\phi_T = \arcsin\left(\frac{\hat{r}_T}{|\hat{H}_T|}\right)$$

$$\Delta\phi_Z = \arcsin\left(\frac{\hat{r}_Z}{|\hat{H}_Z|}\right),$$

where n is twice the number of independent spectral estimates used (200 for the atmospheric data); $F_{m,n}$ is the percentage of an F distribution; and $\hat{\phi}$, $\hat{S}_T$, and $\hat{S}_Z$ are the estimates of the phase angle and square root of the power spectrum of T and Z.

To be 90% certain that ϕ is within 30° of its estimate, $|\gamma|$ must be above 0.30, 0.53, and 0.58 for atmospheric observations, GCM–CLIMO, and GCM–FLAT, respectively. (Recall that fewer seasons of GCM simulations were analyzed.) It should be noted that we are testing for significant vertical tilt rather than a statistically significant relationship. This is more demanding. For example, if the phase angle were 20° in the atmospheric observations, then a significant relationship exists if $|\gamma| > 0.16$ (90% confidence level); however, the sign of the tilt requires a more demanding condition: $|\gamma| > 0.41$.

5. Results

To find the vertical tilts, we first computed $\hat{H}_Z$ from (5). In Figs. 1 and 2, ϕ_Z is shown for 20 winters at 50°N for $k = 1$ and 3. We find the eastward-moving waves (positive frequency) have statistically significant westward tilts (negative ϕ_Z). For the westward-moving waves, the tilt is eastward for $k = 1$. However, this tilt is of marginal significance. For $k = 3$ (Fig. 2), we find no significant tilts for westward-moving waves.

These results are consistent with studies mentioned in section 2 if we account for our larger sample size. If only 2 years of data were used, the angular errors would be 3.5 times larger. With smaller sample size, we would have to conclude that high wavenumber (e.g., $k = 8$), eastward-moving waves have a westward tilt. The other waves would be indistinguishable from equivalent barotropic waves.

We also calculated the vertical tilt from ϕ_T. In Figs. 3 and 4, ϕ_T is shown for $k = 1$ and 3 averaged over 20 winters. Here, we clearly see statistically significant westward tilts for eastward-moving waves and eastward tilts for westward-moving waves with $f < 0.2$ cpd. The structure and significance were similar for the other computed zonal wavenumbers (up to $k = 8$). The results for summer ϕ_T (not shown) were similar except the eastward tilts were much weaker and often not statistically significant (They would be significant if we have averaged over a larger frequency window.)

The advantage of the first method, the cross spectrum of $\hat{Z}$ at 200 and 500 mb, is that it gives a direct estimate of the magnitude of the vertical tilt. The second method is more sensitive but relies on hypsometric equation to give the sign of the vertical tilt. The second method can, however, be used to estimate the magnitude of the vertical tilt. If we neglect the vertical shear

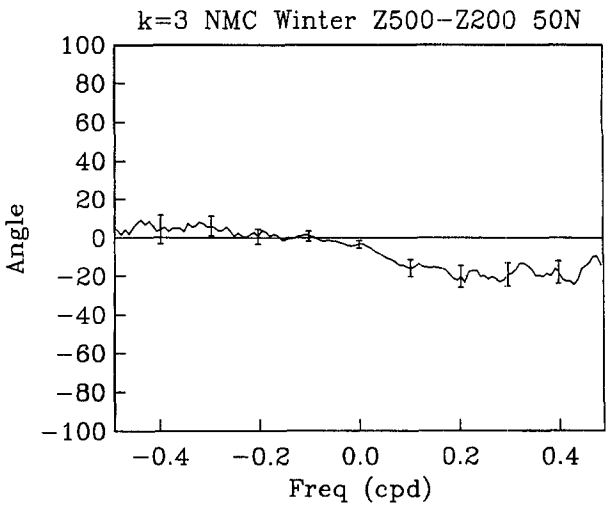

FIG. 2. Same as Fig. 1, except $k = 3$.

of the basic state, then a vertically propagating wave has structure of

$$\Psi = \exp(ikx + ily + imz - z/2H_0),$$

where H_0 is the scale height. Since T is proportional to $\partial\Psi/\partial Z$, we find $\phi_T = \arctan(2mH_0)$. Hence, $m = \tan(\phi_T)/2H_0$. Assuming that the 200- and 500-mb levels are 6.5 km apart, the expected phase shift between the two levels is

$$\phi_Z = \delta_z \cdot m = 6.5 \times 10^3 \text{ m}$$

$$\phi_Z = 6.5 \times 10^3 \tan(\phi_T)/2H_0.$$

Assuming $H_0 = 9$ km gives

$$\phi_Z = 0.36 \tan(\phi_T).$$

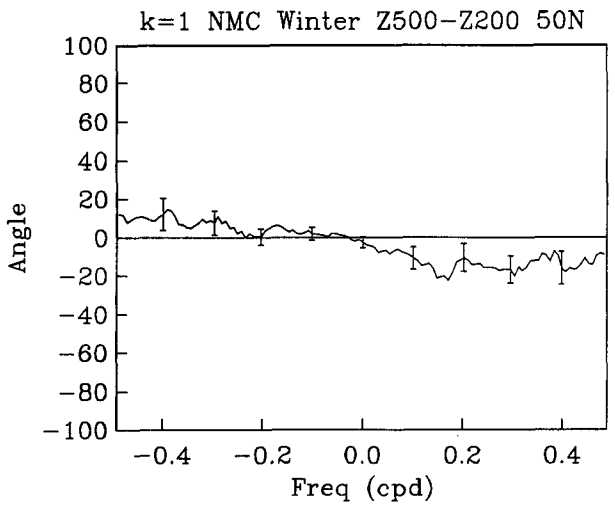

FIG. 1. Phase angle, ϕ_Z, between the $k = 1$ geopotential at 500 and 200 mb (50°N and winter). A positive phase angle indicates an eastward vertical tilt.

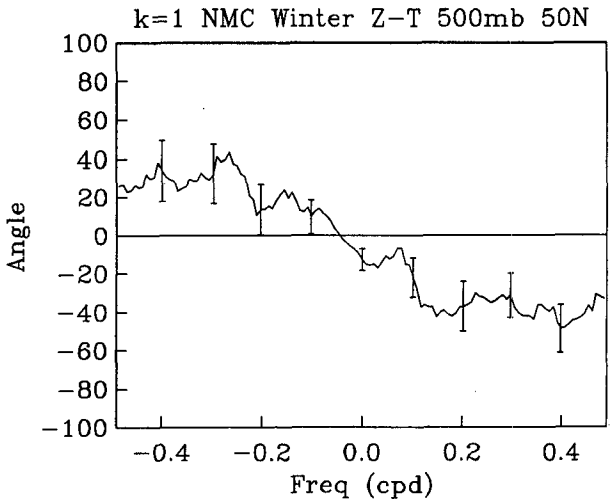

FIG. 3. Phase angle, ϕ_T, between the $k = 1$ geopotential and temperature waves at 500 mb (50°N and winter). A positive phase angle indicates an eastward vertical tilt.

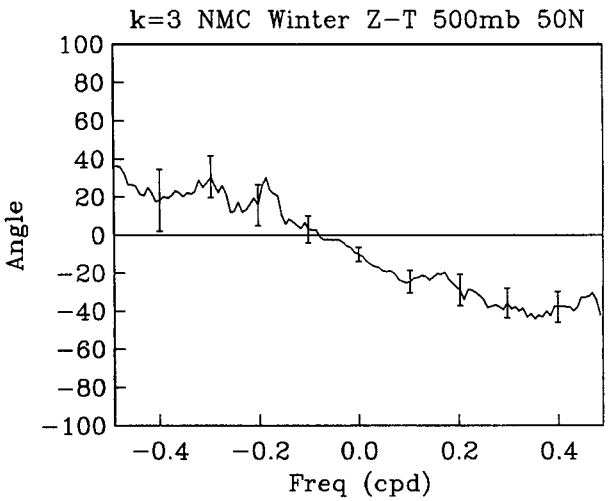

FIG. 4. Same as Fig. 2, except $k = 3$.

The above relationship appears to be consistent with the observations. For example, ϕ_T is about 30° for frequencies between −0.4 and −0.3 cpd (Fig. 3). The above formula gives $\phi_Z = 0.21$ or 12°, which is a good estimate of the observed ϕ_Z at the same frequencies (Fig. 1).

In summary, two methods were used to calculate the vertical tilts in the troposphere. The cross-spectral analysis of $\tilde{Z}$ at 200 and 500 mb showed a westward tilt for eastward-moving waves and a statistically insignificant eastward tilt for westward-moving waves ($f < -0.2$ cpd). On the other hand, the cross-spectral analysis of $\tilde{Z}$ and $\tilde{T}$ was more sensitive. The eastward tilts were now statistically significant. Using a simple analysis, the magnitude of the vertical tilt was estimated and found to be consistent with the direct calculations of the first method.

6. Discussion of observed tilts

The eastward-tilting waves cannot be explained by a linear instability of the zonal flow. The semicircle theorem for quasi-geostrophic flow (Pedlosky 1987) is

$$U_{\min} - \frac{\beta}{2(k^2 + l_{\min}^2)} \leqslant c \leqslant U_{\max},$$

where $U_{\min}$ and $U_{\max}$ are the minimum and maximum zonal winds of the basic state, c is the phase speed, and $l_{\min}$ is the minimum meridional wavenumber allowed by the geometry. The semicircle theorem sets bounds on the phase speed of the unstable waves.

Consider the case: $k = 1$, $f = -0.4$ cpd, which shows a strong eastward tilt during winter (Fig. 3). During winter $U_{\min} \approx -10$ m s^{-1} and, assuming $l_{\min} \approx k$:

$$c = 2\pi R_{\text{earth}} \cos(\theta) f \approx -120 \text{ m s}^{-1}$$

$$U_{\min} - \frac{\beta}{2(k^2 + l_{\min}^2)} \approx -70 \text{ m s}^{-1}.$$

Therefore, c is too small to be associated with a linear instability of the zonal flow. Granted, higher wavenumbers and lower frequencies may be unstable by the semicircle theorem, but if we assume that the eastward-tilting waves are from one source, then the source is not the linear instability of a zonal flow.

Perhaps the eastward-tilting waves are artifacts of our Fourier decomposition (1). For example, standing waves, such as $\cos(\omega t)\exp(ikx + ily + imz)$, decompose into eastward- and westward-moving waves $\frac{1}{2}\exp(ikx + ily + imz - i\omega t) + \frac{1}{2}\exp(ikx + ily + imz + i\omega t)$. However, the vertical tilt of these waves is identical. Therefore, standing waves produce phase angles that are symmetric about the zero frequency. This is unlike the data that is more antisymmetric (Figs. 3 and 4). In addition, one might expect that the standing waves have a slight westward tilt like the stationary waves during winter. This would suggest that standing-wave contamination would produce westward tilts. For the other case of a standing wave with no vertical tilt, $\cos(mz)\exp(ikx + ily)\cos(\omega t)$, we find that this wave decomposes into $\frac{1}{4}\exp(ikx + ily + imz - i\omega t) + \frac{1}{4}\exp(ikx + ily + imz + i\omega t) + \frac{1}{4}\exp(ikx + ily - imz + i\omega t) + \frac{1}{4}\exp(ikx + ily - imz - i\omega t)$. In this case, our analysis would find no meridional heat flux at any frequency, and consequently no vertical tilt as expected. These preceding arguments suggest that contamination by standing waves is not responsible for the observed eastward tilts.

Unexpected tilts were found in our analysis of NMC data. Perhaps the eastward tilts are caused by the analysis scheme, insufficient data over the oceans, or even solar tides. Since these possibilities do not occur in CCM1, we calculated the vertical tilts of the control GCM simulation, GCM-CLIMO. As seen in Fig. 5, the GCM reproduces the observed eastward tilts, although the angles are larger in magnitude and are nois-

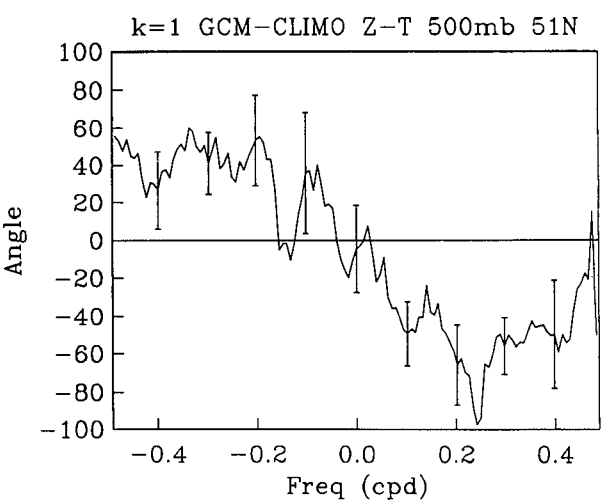

FIG. 5. Same as Fig. 3, except for 51.1°N and GCM-CLIMO.

ier. The noise is due to the smaller sample size. Nevertheless, the ability of the GCM to simulate eastward tilts is important because it eliminates poor data as a source of the eastward tilts, and it allows us to use the GCM as a tool to understand the tilts.

Determining the meridional structure of eastward-tilting waves can be difficult because of the scarcity of observations in the tropics and Southern Hemisphere. To overcome this difficulty, we analyzed GCM–CLIMO. We found that the eastward tilts were stronger and more statistically significant in the northern midlatitudes than the polar regions. In the tropics, the statistically significant tilts disappeared except for a few isolated frequencies (not shown). In the southern midlatitudes, the eastward tilt reappeared although it was much weaker than in the northern midlatitudes. Finally, no evidence of an eastward tilt in the sourthern polar region was found.

7. Theory

In $\log P$ coordinates, the linear potential vorticity equation with a simple linear dissipation added can be written as (see Dickinson 1980)

$$\left(\frac{\partial}{\partial t} + \epsilon + U\frac{\partial}{\partial x}\right)\Delta\psi + \beta_{\text{eff}}\frac{\partial\psi}{\partial x} = 0, \qquad (6)$$

where

$$z = \ln(P_0/P)$$

$$\Delta \equiv \left(\frac{\partial^2}{\partial x^2} + \frac{\partial^2}{\partial y^2} + \lambda^2\frac{\partial^2}{\partial z^2} - \alpha^2\right)$$

$$\lambda^2 = \frac{f^2}{S}$$

$$S = g\left(\frac{RH}{C_P} + \frac{\partial H}{\partial Z}\right)$$

$$H = \frac{RT}{g}$$

$$\alpha^2 = \frac{\partial^2\lambda}{\partial z^2}\lambda - \frac{\partial\lambda}{\partial z}\lambda + \frac{1}{4}\lambda^2$$

$$\Psi = \frac{gh}{f} = \lambda^{-1}\exp(z/2)\psi,$$

and where the other symbols have their conventional meaning. For a plane wave, $\exp(ikx + ily + imz - i\omega t)$:

$$\lambda^2\frac{\partial^2\psi}{\partial z^2} + \left(\frac{\beta_{\text{eff}}}{U - c - i\epsilon/k} - k^2 - l^2 - \alpha^2\right)\psi = 0.$$

When the dissipation is zero ($\epsilon = 0$), the quantity within parentheses determines whether the disturbance is trapped or vertically propagating. If

$$U_C \equiv \frac{\beta_{\text{eff}}}{k^2 + l^2 + \alpha^2},$$

then the solution under the condition $0 < (U - c) < U_C$ is wavy and vertically propagating. If $U_C < (U - c)$, the solution is exponential with height and is vertically trapped.

Using typical values, Dickinson (1980) suggested that U_C was approximately 75, 43, and 25 m s^{-1} for zonal wavenumbers 1 through 3, respectively. On the other hand, a typical eastward-tilting wave has a frequency of -0.4 cpd, which implies that c is -120, -60, and -40 m s^{-1} for wavenumbers 1 through 3. Therefore, $U_C < (U - c)$ and the eastward-tilting waves are in the regime where the waves are exponential with height.

In the inviscid theory, eastward-tilting waves should not tilt because m is imaginary. However, this difference between theory and observations disappears in a dissipative system. Suppose we add a small amount of dissipation ($\epsilon \ll 1$) and include a wave source of frequency ω and wavenumber (k, l) outside the region of interest. After the transients have disappeared, the flow will oscillate at frequency ω. The dispersion relationship can be used to find m for motions forced by this wave source. For frequencies typical of the eastward-tilting wave (i.e., $U_C < U - c$), a Taylor series expansion about the small parameter ϵ gives

$$m_0 = i\lambda^{-1}\left(-\frac{\beta_{\text{eff}}}{U - c} + k^2 + l^2 + \alpha^2\right)^{1/2}$$

$$m = \pm m_0 \pm \frac{i\epsilon\beta_{\text{eff}}}{2\lambda^2(U - c)^2 m_0 k} + O(\epsilon^2). \qquad (7)$$

The first solution (positive sign) for m is bottom trapped with a westward vertical tilt. Here, the wave source is below the region of interest. The energy propagates upward in order to balance the dissipation and maintain a steady-state solution. The other solution of (7) has an eastward vertical tilt and grows exponentially upward. The wave source must be above the region of interest, and energy must propagate downward. Hence, even in the regime of the eastward-tilting waves, energy propagation can be determined from the vertical tilts.

The previous argument is easily made more rigorous by calculating the pressure-work term $\overline{P'w'}$. If the term is positive, then energy is moving upward. Simple calculations show that this term is negative for the eastward-tilting waves as long as $(U - c)$ is positive. Therefore, the eastward-tilting waves are propagating energy downward.

In the following paragraphs, we will show that a simple nonlinear forcing can produce eastward-tilting waves. Consider a flow in a flat channel forced by a meridional gradient in heating. Assuming the gradient is strong enough, baroclinic waves will grow and transport heat northward. Eventually the flow will equilibrate, and we should see baroclinic waves (Ψ_{BC}), which propagate eastward and have westward vertical tilts. These waves should have length and time scales characteristic of baroclinic instability. Now suppose we add

a small amount of topography. The zonal flow (Ψ_Z) will interact with the topography to produce stationary waves (Ψ_{ST}). For our problem, we will assume that Ψ_{ST} is equivalent barotropic. The various waves will exhibit nonlinear interactions; however, only the interaction between Ψ_{ST} and Ψ_{BC} will be considered. The linear perturbation (ψ') forced by Ψ_{ST} and Ψ_{BC} is governed by

$$\left(\frac{\partial}{\partial t} + U\frac{\partial}{\partial x}\right)\Delta\psi' + \beta_{\text{eff}}\frac{\partial\psi'}{\partial x} = -J(\Psi_{ST}, \Delta\Psi_{BC}) - J(\Psi_{BC}, \Delta\Psi_{ST}). \quad (8)$$

For our simple theory, we will assume that ψ' is small and only consider the interaction between two waves from the spectrum of waves. Therefore, let $\Psi_{BC} = \phi_{BC} \times \exp(i\vec{K}_{BC}\cdot\vec{x} - i\omega_{BC}t)$ where $\vec{K}_{BC} = (k_{BC}, l_{BC}, m_{BC})$. In order that the wave propagates eastward and tilts westward, we will require that k_{BC}, $\text{Re}(m_{BC})$, and ω_{BC} are greater than zero. Let the stationary wave be $\Psi_{ST} = \phi_{ST}\exp(i\vec{K}_{ST}\cdot\vec{x})$, where $\vec{K}_{ST} = (k_{ST}, l_{ST}, m_{ST})$, k_{ST} is positive, and, for a barotropic wave, $\text{Re}(m_{ST})$ is zero. With these forms, the forcing in (8) can be rewritten as $F_1 + F_2$, and the linearity of the problem can be used to decompose the solution into two parts:

$$\psi' = \psi_1 + \psi_2,$$

where

$$\left(\frac{\partial}{\partial t} + U\frac{\partial}{\partial x}\right)\Delta\psi_1 + \beta_{\text{eff}}\frac{\partial\psi_1}{\partial x} = F_1 \quad (9)$$

$$\left(\frac{\partial}{\partial t} + U\frac{\partial}{\partial x}\right)\Delta\psi_2 + \beta_{\text{eff}}\frac{\partial\psi_2}{\partial x} = F_2 \quad (10)$$

$$F_1 + F_2 = -J(\Psi_{ST}, \Delta\Psi_{BC}) - J(\Psi_{BC}, \Delta\Psi_{ST})$$

$$F_1 = A\phi_{BC}\phi_{ST}\exp(i(\vec{K}_{ST} + \vec{K}_{BC})\cdot\vec{x} - i\omega_{BC}t)) \quad (11)$$

$$F_2 = -A\phi^*_{BC}\phi_{ST}\exp(i(\vec{K}_{ST} - \vec{K}_{BC})\cdot\vec{x} - i\omega_{BC}t))$$

$$A = \frac{1}{2}(k_{BC}^2 + l_{BC}^2 + m_{BC}^2 - k_{ST}^2 - l_{ST}^2 - m_{ST}^2) \times (k_{BC}l_{ST} - l_{BC}k_{ST}). \quad (12)$$

After the transients have disappeared, ψ_1 and ψ_2 must have the same phase speed and horizontal wavenumbers as their respective forcings, F_1 and F_2. Therefore, ψ_1 will have a phase speed of $(k_{ST} + k_{BC})/\omega_{BC}$ [see (11)], which is positive. Since ψ_1 propagates eastward, it cannot explain the eastward-tilting waves that move westward. On the other hand, F_2 has a phase speed of $(k_{BC} - k_{ST})/\omega_{BC}$ [see (12)]. Since ψ_{BC} and ψ_{ST} are elements of a spectrum of waves, various combinations will produce both positive and negative phase speeds. In particular, combinations of ψ_{BC} and ψ_{ST}, which have $k_{BC} < k_{ST}$, force waves with negative phase speeds. While stationary waves with $k_{ST} < k_{BC}$ have larger amplitudes, their nonlinear forcings have a positive phase speed and do not force westward-moving waves. Therefore, let us examine combinations of waves where $k_{BC} < k_{ST}$. After the transients have disappeared, ψ_2 will have the same horizontal wavenumber and frequency as the forcing:

$$k_2 = k_{ST} - k_{BC}$$

$$l_2 = l_{ST} - l_{BC}$$

$$\omega_2 = -\omega_{BC}. \quad (13)$$

Neglecting $\partial_{m_2}/\partial z$, (10) can be rewritten as

$$\psi_2 = -\frac{iF_2}{k_2(\beta_{\text{eff}} + (U - c_2)\Delta_2)}$$

$$\Delta_2 = -(k_2^2 + l_2^2 + \alpha^2 + \lambda^2 m_2^2). \quad (14)$$

The vertical wavenumber can be found by taking the vertical derivative of (14) and again neglecting $\partial m_2/\partial z$:

$$i(m_{BC} - m_{ST})F_2 = ik\frac{\partial U}{\partial z}\Delta_2\psi_2 - m_2k_2((U - c_2)\Delta_2 + \beta_{\text{eff}})\psi_2.$$

Using (10), we get

$$m_2 = -m_{BC} + m_{ST} - \frac{k\Delta_2\psi_2}{F_2}\frac{\partial U}{\partial z}$$

or

$$m_2 = -m_{BC} + m_{ST} + i\frac{\partial U}{\partial z}\frac{\beta_{\text{eff}}\Delta_2 + (U - c_2)|\Delta_2|^2}{|\beta_{\text{eff}} + (U - c_2)\Delta_2|^2}. \quad (15)$$

Let us assume that the stationary wave has little tilt; that is, $\text{Re}(m_{ST})$ is small. Then if the shear is small ($\partial U/\partial z \ll Um_{BC}$), or if $\text{Im}(m_2)$ is small, $\text{Re}(m_2) \approx -\text{Re}(m_{BC})$. This implies that the forced wave ψ_2 must have an eastward vertical tilt since $\text{Re}(m_{BC})$ and k_2 are both positive.

This forced wave is consistent with the observed eastward-tilting waves. Its predicted frequency (13) is independent of wavenumber as observed. In addition, the $k = 8$ energy spectrum peaks at 0.3 cpd, and -0.3 cpd is a typical frequency for an eastward-tilting wave.

The theoretical relation $\text{Re}(m_2) \approx -\text{Re}(m_{BC})$ is also consistent with observations. The phase angle between the geopotential field is $\phi_Z = \text{Re}(m)\Delta z$, where Δz is the height difference of the two levels. Since $\text{Re}(m_2) \approx -\text{Re}(m_{BC})$, the phase angle of the eastward-tilting waves should be the negative of the more unstable baroclinic waves. This is consistent with observations. For example, the ϕ_Z for $k = 1, 2, 3, 4$ at $f = -0.3$ cpd is $8 \pm 6°$, $3 \pm 6°$, $6 \pm 6°$, and $10 \pm 6°$, respectively. The phase angle for a corresponding baroclinic wave ($k = 8$ at $f = 0.3$) is $-9 \pm 3°$, which is approximately equal to the negative of the eastward phase angles. Other properties of the observations are consistent with

the theory. For example, we found that the eastward-tilting waves were stronger in winter than in summer. This is consistent with the standing and transient eddies being stronger during winter (Oort 1983). Previously it was found that the eastward-tilting waves are weaker in the tropics and polar latitudes. Again, this could be explained by the weaker standing and transient eddies outside of the midlatitudes.

We have ignored ψ_1, the wave forced by F_1. From (9) and (11), it can be deduced that ψ_1 should propagate eastward with a frequency of ω_{BC} and have a westward vertical tilt. However, the importance of ψ_1 is debatable. At $k = 8$, ψ_1 will have the same phase speed as the baroclinically unstable waves, which are much stronger. Hence, ψ_1 will be undetectable. At $k = 1$, ψ_1 will have an eastward phase speed too large for a linear instability of a zonal flow (a 0.4-cpd wave will be linearly stable by the semicircle theorem). However, ψ_1 could be confused with the most unstable normal mode of the nonzonal climatological flow. Theory for the instability of a nonzonal flow (Ebisuzaki 1989) suggests that the most unstable modes will have a structure locally resembling that arising from the instability of a zonal flow. The normal mode instability will have a local wavelength and amplitude that are functions of position and have energy in many zonal modes all with the same frequency ω_{BC}. The long-wavelength zonal modes will have a westward tilt like ψ_1 and a similar frequency. Therefore, ψ_1 could be confused with the normal mode instability of the climatological flow. In addition, ψ_1 could be confused with ψ_2 when $k_{ST} < k_{BC}$. Under this condition, ψ_2 would tilt westward and have the frequency of ω_{BC}. In addition, $|\psi_2|$ should be stronger than $|\psi_1|$ because the observed $|\Psi_{ST}|$ tends to be smaller for larger k. Therefore, the observed westward tilts of the eastward-propagating $k = 1$ waves have at least three possible sources, and any tilts cannot be attributed to ψ_1.

8. Results of GCM–FLAT

In the previous section, our explanation of the eastward tilts was presented. Our theory appears consistent with the observations. As another test of the theory, we ran a GCM that has no source of stationary waves. If the theory is correct, then eastward-tilting waves should not form.

With the altered surface topography, the zonal winds were much different in GCM–FLAT. Nevertheless, we can still examine the phase angles. It was found that the phase angles ($k = 1$ is shown in Fig. 6) for the westward-moving waves ($f < 0$) were clustered about zero. After considering the observational error, no evidence was found for eastward-tilting waves in GCM–FLAT as the westward-moving waves are nearly equivalent barotropic. Since our theory requires stationary waves to produce the eastward-tilting waves, the lack of the eastward-tilting waves is consistent with the theory.

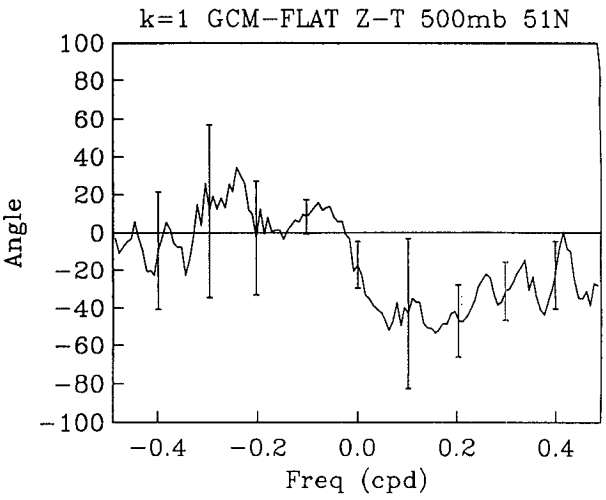

FIG. 6. Same as Fig. 3, except for 51.1°N and GCM-FLAT.

9. Discussion

In summary, we have used spectral analysis techniques to find the vertical tilt of waves, an important consideration in the dynamics of the atmosphere. The vertical tilts were calculated as a function of zonal wavenumber, frequency, and latitude with an emphasis on the northern midlatitude troposphere during winter. We found that the eastward-propagating waves in the midlatitude troposphere tilted westward with height, consistent with a poleward heat flux, an upward group velocity, and the dominant role of baroclinic instability. The westward-propagating waves, on the other hand, tilted eastward, except for the frequencies lower than 0.1 cpd, which were nearly barotropic.

We also found that CCM1, a general circulation model, could simulate the eastward-tilting waves. The CCM1 is not unique, because Tokioka and Noda (1986) found that the Meteorological Research Institute (MRI) GCM had westward-traveling waves that had a southward heat flux at 700 mb. We took advantage of the CCM1 to further examine these waves, finding that eastward tilts in CCM1, and presumably in the atmosphere, were a midlatitude phenomenon, stronger during winter.

We hypothesized that the eastward-tilting waves were the forced response to nonlinearities involving cyclone-scale waves and stationary waves forced by orography and diabatic heating. The solution to our simple theory had phase speeds and vertical tilts consistent with the observations. We then ran the CCM1 with a flat, uniform topography. According to our theory, the eastward tilts should disappear because the simulation should have no stationary waves, and, indeed, the eastward tilts did disappear.

If the interaction does indeed force these waves, we have found one mechanism that puts energy into the frequency and zonal-wavenumber band that includes

some of the global Rossby waves. Consequently, our mechanism is potentially a source of these waves. This is consistent with Hayashi and Golder (1983a) and Tokioka and Noda (1986), who found that the westward-propagating waves are weaker in GCM simulations where the mountains were removed. In addition, this theory suggests that nonlinear interactions can transfer energy from the eastward-moving waves and increase the energy in the westward-moving waves. This again is consistent with the GCM simulations of Hayashi and Golder (1983a, 1983b) and Tokioka and Noda (1986), who noted an increase of energy in the eastward-moving waves when mountains were removed.

In section 7, we emphasized the interactions involving waves with $k_{ST} > k_{BC}$ because they force waves with an eastward vertical tilt. Nonlinear interactions involving stationary and baroclinic waves that satisfy $k_{BC} > k_{ST}$ are stronger because $|\psi_{ST}|$ is larger for lower wavenumbers. However, we did not consider them because they force eastward-moving waves with a westward vertical tilt, which would be indistinguishable from waves of other sources. Nevertheless, interactions of both types should occur when we have a spectrum of waves. The interactions involving waves where $k_{BC} > k_{ST}$ should transfer energy from the baroclinically unstable waves and increase the energy in the longer, eastward-moving waves. There is a suggestion that this may be occurring in Tokioka and Noda (1986).

Acknowledgments. I would like to thank Dr. B. Saltzman for his help, Dr. J. Park for answering my questions on statistics, and Dr. R. Oglesby for his essential help with using the CCM1. This research was supported by the Global Scale Atmospheric Processes Research Program of NASA under Grant NAG8-785, and the GCM simulations were done at the National Center for Atmospheric Research, which is sponsored by the National Science Foundation.

REFERENCES

Böttger, H., and K. Fraedrich, 1980: Disturbances in the wavenumber-frequency domain observed along 50°N. *Contrib. Atmos. Phys.*, **53**, 90–106.

Deland, R. J., 1973: Spectral analysis of traveling planetary scale waves: Vertical structure in the middle latitudes of Northern Hemisphere. *Tellus,* **25**, 355–373.

Dickinson, R. E., 1980: Planetary waves: Theory and observation. *Orographic Effects in Planetary Flows.* GARP Publ. Ser. No. 23, WMO-ICSU, Geneva, 53–84.

Ebisuzaki, W., 1989: Interactions between long and synoptic-scale waves. Part I: Instability of a nonzonal flow. *J. Atmos. Sci.,* **45,** 411–449.

Hayashi, Y., 1982: A generalized method of resolving disturbances into progressive and retrogressive waves by space Fourier and time cross-spectral analyses. *J. Meteor. Soc. Japan,* **49,** 125–128.

——, and D. G. Golder, 1983a: Transient planetary waves simulated by GFDL spectral general circulation models. Part I: Effects of mountains. *J. Atmos. Sci.,* **40,** 941–950.

——, and ——, 1983b: Transient planetary waves simulated by GFDL spectral general circulation models. Part II: Effects of nonlinear energy transfer. *J. Atmos. Sci.,* **40,** 951–957.

Madden, R. A., 1979: Observations of large-scale traveling Rossby waves. *Rev. Geophys. Space Phys.,* **17,** 1935–1949.

——, and P. Speth, 1989: The average behavior of large-scale westward traveling disturbances evident in the Northern Hemisphere geopotential heights. *J. Atmos. Sci.,* **46,** 3225–3239.

Mass, C. F., H. J. Edmon, H. J. Friedman, N. R. Cheney and E. R. Recker, 1987: The use of compact discs for the storage of large meteorological and oceanographic datasets. *Bull. Amer. Meteor. Soc.,* **68,** 1556–1558.

Mechoso, C. R., and D. L. Hartmann, 1982: An observational study of traveling planetary waves in the Southern Hemisphere. *J. Atmos. Sci.,* **39,** 1921–1935.

Oort, A., 1983: Global Atmospheric Circulation Statistics, 1958–1973. NOAA Prof. Paper 14, Washington, D.C., 180 pp.

Otnes, R. K., and L. Enochson, 1978: *Applied Time Series Analysis. Vol. 1: Basic Techniques.* John Wiley & Sons, 444 pp.

Pedlosky, J., 1987: *Geophysical Fluid Dynamics.* Springer-Verlag, 624 pp.

Pratt, R. W., and J. M. Wallace, 1976: Zonal propagation characteristics of large-scale fluctuations in the midlatitude troposphere. *J. Atmos. Sci.,* **33,** 1184–1194.

Salby, M. L., 1981: Rossby normal modes in nonuniform background configurations. Part II: Equinox and solstice conditions. *J. Atmos. Sci.,* **38,** 1827–1840.

——, 1984: Survey of planetary-scale traveling waves: The state of theory and observations. *Rev. Geophys. Space Phys.,* **22,** 209–236.

Sato, Y., 1977: Transient planetary waves in the winter stratosphere. *J. Meteor. Soc. Japan,* **55,** 89–106.

Shutts, G. J., 1978: Quasi-geostrophic planetary wave forcing. *Quart. J. Roy. Meteor. Soc.,* **104,** 331–350.

Tokioka, T., and A. Noda, 1986: Effects of large-scale orography on January atmospheric circulation: A numerical experiment. *J. Meteor. Soc. Japan,* **64,** 819–839.

Venne, D. E., 1989: Normal-mode Rossby waves observed in the wavenumber 1–5 geopotential fields of the stratosphere and troposphere. *J. Atmos. Sci.,* **46,** 1042–1056.

Williamson, D. L., J. T. Kiehl, V. Ramanathan, R. E. Dickinson and J. J. Hack, 1987: Description of NCAR Community Climate Model (CCM1). NCAR Tech. Note NCAR/TN-285+STR, 112 pp. [Available from the National Center for Atmospheric Research, Boulder, CO.]

Williamson, G. S., and D. L. Williamson, 1987: Circulation statistics from seasonal and perpetual January and July simulations with the NCAR Community Climate Model (CCM1): R15. NCAR Tech. Note NCAR/TN-302+STR, 199 pp. [Available from the National Center for Atmospheric Research, Boulder, CO.]